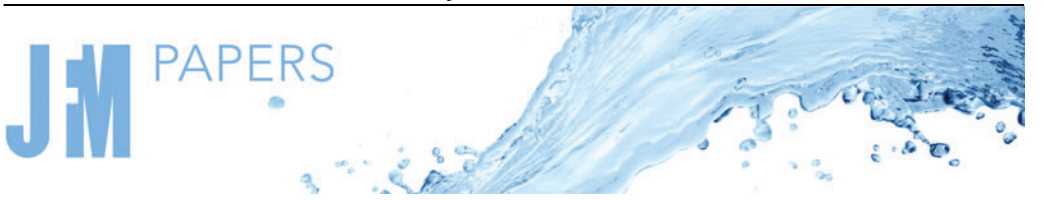
J. Fluid Mech. (2024), *vol*. 989, A8, doi:10.1017/jfm.2024.490



Stability of triple-diffusive convection in a vertical porous layer

B.M. Shankar[1],† **and I.S. Shivakumara**[2]

[1]Department of Mathematics, PES University, Bangalore 560 085, India

[2]Department of Mathematics, Bangalore University, Bangalore 560 056, India

(Received 16 November 2023; revised 31 March 2024; accepted 12 May 2024)

The classical Gill's problem, focusing on the stability of thermal buoyancy-driven convection in a vertical porous slab with impermeable isothermal boundaries, is studied from a different perspective by considering a triple-diffusive fluid system having different molecular diffusivities. The assessment of stability/instability of the basic flow entails a numerical solution of the governing equations for the disturbances as Gill's proof of linear stability falls short. The updated problem formulation is found to introduce instability in contrast to Gill's original set-up. A systematic examination of neutral stability curves is undertaken for KCl–NaCl–sucrose and heat–KCl–sucrose aqueous systems which are found to exhibit an anomalous behaviour on the stability of base flow. It is found that, in some cases, the KCl–NaCl–sucrose system necessitates the requirement of four critical values of the Darcy–Rayleigh number to specify the linear stability criteria ascribed to the existence of two isolated neutral curves positioned one below the other. Conversely, the heat–KCl–sucrose system demands only two critical values of the Darcy–Rayleigh number to decide the stability of the system. The stability boundaries are presented and the emergence of a travelling-wave mode supported back and forth with stationary modes is observed due to the introduction of a third diffusing component. In addition, some intriguing outcomes not recognized hitherto for double-diffusive fluid systems are manifested.

1. Introduction

The pioneering paper by Gill (1969) has provided an interesting analytical proof that convection due to thermal buoyancy in a vertical porous layer bounded by isothermal impermeable walls is always stable for all infinitesimal perturbations. The obtained results offered significant justification for the use of insulating porous materials in buildings, obviating the necessity for air gaps. The work by Gill (1969) was further extended by

† Email address for correspondence: bmshankar@pes.edu

© The Author(s), 2024. Published by Cambridge University Press

https://doi.org/10.1017/jfm.2024.490 Published online by Cambridge University Press

other authors including additional effects such as the Prandtl–Darcy number (Rees 1988), lack of local thermal equilibrium between the fluid and the solid phases (Rees 2011) and the nonlinearity of the perturbation dynamics (Straughan 1988; Scott & Straughan 2013). These investigations collectively furnished compelling evidence that the fluid flow stability established by Gill remains valid. On the other hand, the possibility of Gill's problem becoming unstable was established by taking into account temperature-dependent viscosity (Kwok & Chen 1987; Shankar, Nagamani & Shivakumara 2023), vertical boundaries to be permeable (Barletta 2015), boundary and inertia effects (Shankar, Kumar & Shivakumara 2017), viscoelasticity of the fluid (Shankar & Shivakumara 2017; Lazzari, Celli & Barletta 2021), maximum density property with time-dependent velocity term in Darcy's law (Naveen, Shankar & Shivakumara 2020), horizontal heterogeneity in permeability (Shankar & Shivakumara 2022), sandwiched vertical porous slab (Barletta *et al.* 2022) and the Prandtl–Darcy number with internal heating (Nagamani, Shankar & Shivakumara 2023).

Numerous fluid dynamical systems manifest in nature and various scenarios wherein buoyancy forces instigate the movement of a fluid laden with dissolved minerals through a porous medium. Notably, double-diffusive convection encompasses two interacting species that influence the distribution of fluid density. For instance, this phenomenon might involve two solute concentrations with distinct molecular diffusivities or combinations of heat and solute concentration. The exploration of double-diffusive convection in a fluid-saturated porous medium has remained a vibrant and enduring research domain for numerous decades, owing to its significance and broad-ranging applications across disciplines including oceanography, migration of pollutants through saturated soil, geophysics, astrophysics and engineering (Griffiths 1981; Pritchard & Richardson 2007; Straughan 2015). Comprehensive assessments of the theoretical and empirical analyses pertaining to double-diffusive convection in a porous medium can be found in Cheng (1979) and Nield & Bejan (2017). However, it is noteworthy that investigation into the stability of double-diffusive convection in a vertical porous layer has been relatively limited within the existing literature.

The stability of stationary convective flow in a vertical porous layer saturated with a binary mixture by imposing different temperatures and zero mass flux at the boundaries was considered by Gershuni, Zhukhovitskii & Lyubimov (1976). It has been shown that in the presence of sufficient longitudinal stratification, the flow becomes unstable against thermal–concentration perturbations. Khan & Zebib (1981) furthered this investigation by extending it across all ranges of the salinity Darcy–Rayleigh number. Shankar, Naveen & Shivakumara (2022) delved into the effects of a second diffusing component on the stability of thermal convection in a vertical porous layer. This was done under conditions involving constant but distinct temperatures and solute concentrations at impermeable vertical boundaries. Their findings revealed the formation of closed loops in the neutral stability curves and the enlargement of the instability region with increasing solute/thermal Darcy–Rayleigh number as well as the Lewis number. Overall, the study demonstrated that double-diffusive fluid systems exhibit a significantly more intricate dynamic behaviour in comparison with the conventional single-component system (Gill 1969).

The possibility of fluid dynamical systems in porous media, where fluid density is influenced by three or more stratifying agencies with different molecular diffusivities, cannot be ruled out and, as a result, one can expect multicomponent convection. Degens *et al.* (1973) highlighted the occurrence of double-diffusive convection in geothermal systems, where salinity of comparable concentrations of many salts can trigger convection encompassing multi-diffusing components. Another pertinent example is in contaminant

https://doi.org/10.1017/jfm.2024.490 Published online by Cambridge University Press

transport scenarios (Celia, Kindred & Herrera 1989; Chen *et al.* 1994), where various non-reactive chemical species contribute to contaminant formation. Also, the effects of dyes or small temperature gradients on the accuracy of laboratory experiments on double-diffusive convection in porous media may introduce a third property that affects the density of the fluid. Furthermore, investigating convective instability in mushy layers formed during the solidification of multicomponent alloys holds significance (Anderson & Worster 1996; Guba & Worster 2006). A mushy layer, akin to a porous medium (Phillips 1991), facilitates interstitial melt flow, underscoring the importance of studying multicomponent convection in such contexts. These intricate fluid dynamical systems are also observed in geothermally heated lakes, magmas and their laboratory models. To this end, triple-diffusive convection in a horizontal porous layer has been undertaken by a multitude of researchers (Rudraiah & Vortmeyer 1982; Poulikakos 1985; Tracey 1996; Rionero 2012, 2013; Raghunatha, Shivakumara & Shankar 2018; Shivakumara & Raghunatha 2022 and references therein). Several remarkable departures from those of double-diffusive fluid systems have been found when a third diffusing component is present, particularly for the onset of convection.

In this context, it is pragmatic to contribute further novel findings to the present knowledge on the stability of double-diffusive natural convection in a vertical porous layer by considering a third diffusing component. To the best of our knowledge, such study has not received any attention in the literature. The aim of this paper is to investigate the linear stability of buoyancy-driven convection in a triple-diffusive fluid-saturated vertical porous layer by assuming small-amplitude perturbations of the basic flow. The resulting eigenvalue problem governing the stability of the fluid flow is numerically solved. The topology of neutral curves is outlined systematically and the stability boundary is noted to be significantly more intricate depending on the transport property ratios. It is established that the triple-diffusive fluid systems support several remarkable departures from what occurs in single- and double-diffusive systems. It is observed that more than two critical Darcy–Rayleigh numbers correspond to the linear onset of instability under certain conditions.

2. Mathematical formulation

The stability of buoyancy-driven convection in a triple-diffusive fluid saturating a vertical layer of a Darcy porous medium of width $2h$ is considered as shown in figure 1. The concentration C_i $(i = 1, 2, 3)$ of each individual diffusing component (one of the diffusing mechanisms may be heat) along the right- and left-hand vertical impermeable boundaries is held at different constant value C_{ir} and C_{il}, respectively. The x axis is horizontal and perpendicular to the vertical planes, the z axis is pointing vertically upward and the y axis is horizontal and parallel to the planes. The gravitational acceleration $\boldsymbol{g}$, with modulus g, acts in the downward vertical direction. The porous medium exhibits isotropic and homogeneous characteristics, with negligible influence of viscous dissipation and the absence of volumetric heating. The local thermal equilibrium between the solid and the fluid phases is assumed and the Oberbeck–Boussinesq approximation holds. Besides, the off-diagonal (Soret, Dufour and cross-diffusion) contributions to the fluxes of the stratifying agencies are neglected. The density ρ of an incompressible fluid is assumed to vary linearly in the form

$$\rho = \rho_0 \left[1 - \sum_{i=1}^{3} \alpha_i (C_i - C_{i0}) \right], \tag{2.1}$$

https://doi.org/10.1017/jfm.2024.490 Published online by Cambridge University Press

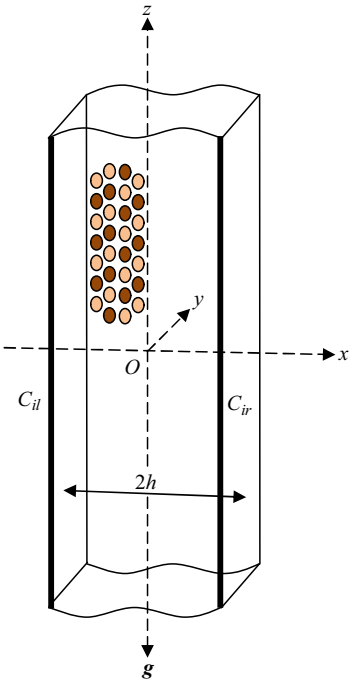


Figure 1. A sketch of the physical model.

where ρ_0 is the reference density at reference solute concentrations $C_{i0} = (C_{il} + C_{ir})/2$ and the coefficients α_i are constants. The governing equations under the above assumptions are

$$\nabla \cdot \boldsymbol{q} = 0, \tag{2.2}$$

$$\nabla p = -\rho_0 \sum_{i=1}^{3} \alpha_i (C_i - C_{i0}) \boldsymbol{g} - \frac{\mu}{K} \boldsymbol{q}, \tag{2.3}$$

$$\varepsilon_i \frac{\partial C_i}{\partial t} + (\boldsymbol{q} \cdot \nabla) C_i = \kappa_i \nabla^2 C_i \quad (i = 1, 2, 3), \tag{2.4}$$

where $\boldsymbol{q} = (u, v, w)$ is the seepage velocity, p is the pressure, μ is the fluid viscosity, K is the permeability, $\varepsilon_i = \varepsilon = \text{const.}$ $(i = 1, 2, 3)$ is the porosity, t is the time and κ_i $(i = 1, 2, 3)$ are the solutal diffusivities. If one of the diffusing components is heat, say the component $i = 1$, then ε_1 in (2.4) stands for the ratio of heat capacities defined as $\varepsilon_1 = [\varepsilon(\rho c)_f + (1 - \varepsilon)(\rho c)_s]/(\rho c)_f$, where $(\rho c)_f$ and $(\rho c)_s$ are the heat capacities of the fluid and the solid matrix, respectively, and its value is assumed to be 1. That is, the effect of the heat capacity of the solid matrix is neglected and this simplification is valid when the solid matrix is composed of low-heat-capacity materials such as metals.

The boundary conditions are

$$\boldsymbol{q} \cdot \hat{i} = 0 \text{ at } x = \pm h, \quad C_i = C_{il} \text{ at } x = -h, \quad C_i = C_{ir} \text{ at } x = h. \tag{2.5a–c}$$

https://doi.org/10.1017/jfm.2024.490 Published online by Cambridge University Press

The quantities are made dimensionless as follows:

$$\boldsymbol{q}^* = \frac{\boldsymbol{q}}{(\kappa_1/h)}, \quad t^* = \frac{t}{(\varepsilon h^2/\kappa_1)}, \quad \nabla^* = h\nabla, \quad p^* = \frac{p}{(\kappa_1\mu/K)}, \quad C_i^* = \frac{C_i - C_{i0}}{(C_{ir} - C_{il})} \quad (i = 1, 2, 3). \tag{2.6a–e}$$

Using (2.6), (2.2)–(2.5) become (after ignoring the asterisks for simplicity)

$$\nabla \cdot \boldsymbol{q} = 0, \tag{2.7}$$

$$\nabla p = \sum_{i=1}^{3} R_i C_i \hat{k} - \boldsymbol{q}, \tag{2.8}$$

$$\frac{\partial C_i}{\partial t} + (\boldsymbol{q} \cdot \nabla) C_i = \frac{1}{Le_i} \nabla^2 C_i \quad (i = 1, 2, 3), \tag{2.9}$$

$$\boldsymbol{q} \cdot \hat{i} = 0, \quad C_i = \pm 1/2 \text{ at } x = \pm 1 \ (i = 1, 2, 3). \tag{2.10}$$

Here, $R_i = \alpha_i g (C_{ir} - C_{il}) hK/\kappa_1 \nu$ and $Le_i = \kappa_1/\kappa_i$ are the Darcy–Rayleigh numbers and the Lewis numbers, respectively, for $i = 1, 2, 3$, while $\nu = \mu/\rho_0$ is the kinematic viscosity of the fluid and $\hat{k}$ is unit vector along the z axis. Given the evident applicability of Squire's theorem (Barletta 2015; Shankar, Shivakumara & Naveen 2021), it has prompted the introduction of the stream function $\psi(x, z, t)$ in the form $u = -\partial\psi/\partial z$; $w = \partial\psi/\partial x$ and consequently the pressure is eliminated by operating curl on the momentum equation, and thus we obtain

$$\left(\frac{\partial^2 \psi}{\partial x^2} + \frac{\partial^2 \psi}{\partial z^2}\right) = \sum_{i=1}^{3} R_i \frac{\partial C_i}{\partial x}, \tag{2.11}$$

$$\frac{\partial C_i}{\partial t} - \frac{\partial \psi}{\partial z}\frac{\partial C_i}{\partial x} + \frac{\partial \psi}{\partial x}\frac{\partial C_i}{\partial z} = \frac{1}{Le_i} \nabla^2 C_i \quad (i = 1, 2, 3). \tag{2.12}$$

The boundary conditions now become

$$\psi = 0, \quad C_i = \pm 1/2 \text{ at } x = \pm 1 \quad (i = 1, 2, 3). \tag{2.13}$$

2.1. *Basic state*

The base flow is assumed to be fully developed, unidirectional, time-independent and laminar. These assumptions reduce (2.11) and (2.12) to ordinary differential equations of the form

$$\frac{\mathrm{d}^2 \psi_b}{\mathrm{d}x^2} = \sum_{i=1}^{3} R_i \frac{\mathrm{d}C_{ib}}{\mathrm{d}x}, \tag{2.14}$$

$$\frac{\mathrm{d}^2 C_{ib}}{\mathrm{d}x^2} = 0 \quad (i = 1, 2, 3), \tag{2.15}$$

where the suffix b serves to denote 'basic flow'. The associated boundary conditions are

$$\psi_b = 0, \quad C_{ib} = \pm 1/2 \text{ at } x = \pm 1 \quad (i = 1, 2, 3). \tag{2.16}$$

https://doi.org/10.1017/jfm.2024.490 Published online by Cambridge University Press

The solution to the basic flow is found to be

$$\psi_b = \frac{(R_1 + R_2 + R_3)}{4}(x^2 - 1), \tag{2.17}$$

$$C_{ib} = \frac{x}{2} \quad (i = 1, 2, 3). \tag{2.18}$$

It may be noted that the nature of the basic velocity profile is not altered due to the consideration of additional solute concentration fields but the additional stratifying agencies change the magnitude of ψ_b.

2.2. *Disturbance equations*

In order to test the stability of the basic flow, the standard procedure is perturbing the system. Accordingly, disturbances of small amplitude are superimposed in the form

$$\psi = \psi_b + \psi', \quad C_i = C_{ib} + C_i' \quad (i = 1, 2, 3), \tag{2.19}$$

where primes serve to denote the perturbation field. Substituting equation (2.19) into (2.11)–(2.13) and linearizing we get (after ignoring the primes for simplicity)

$$\left(\frac{\partial^2 \psi}{\partial x^2} + \frac{\partial^2 \psi}{\partial z^2}\right) = \sum_{i=1}^{3} R_i \frac{\partial C_i}{\partial x}, \tag{2.20}$$

$$\frac{\partial C_i}{\partial t} - DC_{ib}\frac{\partial \psi}{\partial z} + D\psi_b \frac{\partial C_i}{\partial z} = \frac{1}{Le_i}\nabla^2 C_i \quad (i = 1, 2, 3), \tag{2.21}$$

$$\psi = 0 = C_i \text{ at } x = \pm 1 \quad (i = 1, 2, 3), \tag{2.22}$$

where the operator $D = \mathrm{d}/\mathrm{d}x$.

2.3. *Normal modes*

We now focus on the dynamics of normal modes expressed as

$$(\psi, C_i)(x, z, t) = (\Psi, \Phi_i)(x)\, \mathrm{e}^{\mathrm{i}a(z - ct)}, \tag{2.23}$$

with a real wavenumber a and temporal complex eigenvalue $c\ (= c_r + \mathrm{i}c_i)$. We now substitute equation (2.23) into (2.20)–(2.22), which yields the eigenvalue problem

$$(D^2 - a^2)\Psi = \sum_{i=1}^{3} R_i D\Phi_i, \tag{2.24}$$

$$-\mathrm{i}aDC_{ib}\Psi + \mathrm{i}aD\psi_b\Phi_i - \frac{1}{Le_i}(D^2 - a^2)\Phi_i = \mathrm{i}ac\Phi_i \quad (i = 1, 2, 3), \tag{2.25}$$

$$\Psi = \Phi_i = 0 \ (i = 1, 2, 3) \text{ at } x = \pm 1. \tag{2.26}$$

The imaginary part of the eigenvalue, i.e. the growth rate c_i, is an important parameter as it allows one to detect the linear stability ($c_i \leq 0$) or instability ($c_i > 0$) of the basic solution. We could not find a rigorous proof that the solution of (2.24)–(2.26) yields $c_i \leq 0$, as proved by Gill (1969) for a single-diffusing-component system. We may expect that the instability initiates when the parameter R_1 exceeds a threshold value by considering the other governing parameters as given. Thus, the above eigenvalue problem allows one to evaluate numerically the threshold value of R_1 for the onset of instability.

https://doi.org/10.1017/jfm.2024.490 Published online by Cambridge University Press

3. Numerical procedure

To solve the stability eigenvalue problem governed by (2.24)–(2.26), the spectral Chebyshev collocation technique has been employed. Accordingly, the governing equations are discretized along the x direction at the Gauss–Lobatto collocation points of Mth order in the domain $[-1, 1]$. The Gauss–Lobatto points are given as

$$x_j = \cos\left(\frac{\pi j}{M}\right), \quad j = 0, 1, 2, \ldots, M, \tag{3.1}$$

where M represents the order of the base polynomial. These $M + 1$ grid points correspond to the extreme points of the first kind Chebyshev polynomial of degree M:

$$\tau_M(x) = \cos(M\cos^{-1}x). \tag{3.2}$$

Using a truncated Chebyshev series, we construct an interpolating polynomial in terms of unknown field variables at the collocation points. The unknown function $f(x)$ and its derivatives are then approximated in accordance with the values of this function at the collocation points. The Mth-order polynomial representation of function $f(x)$ is presented as follows:

$$f(x) = \sum_{j=0}^{M} h_j(x) f(x_j), \tag{3.3}$$

where the Lagrange interpolant $h_j(x)$ is defined as

$$h_j(x) = \frac{(-1)^{j+1}(1 - x^2)\tau'_M(x)}{M^2 c_j (x - x_j)}, \tag{3.4}$$

with

$$c_j = \begin{cases} 1 & 1 \le j \le M - 1, \\ 2 & j = 0, M, \end{cases} \tag{3.5}$$

and $\tau'_M(x)$ denotes derivative of the Mth-order Chebyshev polynomial. The interpolant $h_j(x)$ also adheres to the Kronecker delta property:

$$h_j(x_k) = \delta_{jk}, \tag{3.6}$$

where δ_{jk} is known as the Kronecker delta symbol. The explicit determination of derivatives of varying orders can be achieved by differentiating equation (3.3). The expressions for the first- and second-order derivatives at the collocation points x_j are provided below:

$$\left.\frac{\mathrm{d}f}{\mathrm{d}x}\right|_j = \sum_{k=0}^{M} D^{(1)}_{jk} f_k, \quad j = 0, 1, \ldots, M, \tag{3.7}$$

$$\left.\frac{\mathrm{d}^2 f}{\mathrm{d}x^2}\right|_j = \sum_{k=0}^{M} D^{(2)}_{jk} f_k, \quad j = 0, 1, \ldots, M. \tag{3.8}$$

https://doi.org/10.1017/jfm.2024.490 Published online by Cambridge University Press

In this context, f_k is essentially just $f(x_k)$. The Chebyshev differentiation matrices $D^{(1)}_{jk}$ and $D^{(2)}_{jk}$ have an order of $(M+1)\times(M+1)$ and are defined as

$$D^{(1)}_{jk} = \begin{cases} \dfrac{c_j(-1)^{k+j}}{c_k(x_j - x_k)} & j \neq k, \\ -\dfrac{x_j}{2(1-x_j^2)} & 1 \leq j = k \leq M-1, \\ \dfrac{2M^2+1}{6} & j = k = 0, \\ -\dfrac{2M^2+1}{6} & j = k = M, \end{cases} \tag{3.9}$$

and $D^{(2)}_{jk} = D^{(1)}_{jm} \cdot D^{(1)}_{mk}$. The comprehensive methodology is extensively elucidated in the books by Canuto *et al.* (1988) and Peyret (2002). The application of this approach to (2.24) and (2.25) gives

$$\sum_{k=0}^{M} D^{(2)}_{jk}\Psi_k - a^2\Psi_j - \sum_{k=0}^{M}\sum_{i=1}^{3} R_i D^{(1)}_{jk}\Phi_{ik} = 0, \tag{3.10}$$

$$-\frac{\mathrm{i}a}{2}\Psi_j + \mathrm{i}a\left[\frac{(R_1+R_2+R_3)}{2}\right]x_j\Phi_{ij} - \frac{1}{Le_i}\left[\sum_{k=0}^{M} D^{(2)}_{jk}\Phi_{ik} - a^2\Phi_{ij}\right]$$
$$= \mathrm{i}ac\Phi_{ij} \quad (i = 1, 2, 3). \tag{3.11}$$

Equations (3.10) and (3.11) are now discretized for inner collocation points ($j = 1$ to M), and the boundary conditions are discretized for $j = 0$ ($x = 1$) and $j = M$ ($x = -1$). This procedure culminates in solving a generalized eigenvalue problem:

$$\boldsymbol{AX} = c\boldsymbol{BX}, \tag{3.12}$$

where c and $\boldsymbol{X}$ are the eigenvalue and the eigenvector of field entities, respectively, while $\boldsymbol{A}$ and $\boldsymbol{B}$ are square and complex matrices of order $(4M+4)\times(4M+4)$. A complex analogue of the QZ algorithm developed by Moler & Stewart (1973) is used to solve the aforementioned eigenvalue problem. The coordinates along the neutral stability curves are determined through an iterative secant method, where either the wavenumber a is held constant while varying R_1, or *vice versa*, with R_1 fixed while modifying a. This iteration continues until the condition $c_i = 0$ is fulfilled within a predefined error threshold. The eigenvalue c is the eigenvalue with the largest imaginary part for the particular type of disturbance in question. The errors associated with a and R_1 at the neutral point are assessed to be below 0.0001 %. The critical values of a and R_1 are established through polynomial interpolation based on data points near the nadir of the neutral curve. The critical Darcy–Rayleigh number $R_{1c} = \min(R^S_{1c}, R^T_{1c})$, where R^S_{1c} and R^T_{1c} are the critical Darcy–Rayleigh numbers for the stationary and the travelling-wave disturbances, respectively.

4. Results and discussion

The results are presented exclusively for a KCl–NaCl–sucrose aqueous system for which $\kappa_1 = 1.6\times10^{-5}$ cm^2 s^{-1}, $\kappa_2 = 1.3\times10^{-5}$ cm^2 s^{-1}, $\kappa_3 = 0.45\times10^{-5}$ cm^2 s^{-1}

https://doi.org/10.1017/jfm.2024.490 Published online by Cambridge University Press

(i.e. $Le_1 = 1$, $Le_2 = 1.2307$, $Le_3 = 3.5555$) and also for an aqueous solution of heat–KCl–sucrose system for which $\kappa_1 = 1.4 \times 10^{-3}$ cm^2 s^{-1}, $\kappa_2 = 1.6 \times 10^{-5}$ cm^2 s^{-1}, $\kappa_3 = 0.45 \times 10^{-5}$ cm^2 s^{-1} (i.e. $Le_1 = 1, Le_2 = 87.5, Le_3 = 311.1111$) (Griffiths 1979). In the former case, it is seen that the Lewis numbers are not far from unity, as is typical of molecular species in molten metals and magmas as well as of laboratory models using salt–sugar solutions. The Darcy–Rayleigh numbers R_2 and R_3 are allowed to vary, while R_1 is taken as a free parameter. The presence of additional diffusing components instils instability on the basic flow and a systematic study of the topology of neutral stability curves has been undertaken by performing linear stability analysis. The neutrally stable configuration is identified by $c_i = 0$ which delimits the boundary between the regions of parametric stability and instability in the (a, R_1) plane.

4.1. *Validation of the code*

To validate the numerical code, we calculate the critical values of R_1, a and c by systematically adjusting the number of collocation points within the sample sets of governing parameters. The findings presented in table 1 indicate that the convergence of the numerical scheme improves as the number of collocation points increases. It is apparent that employing 25 collocation points yields accurate results up to six decimal places for the KCl–NaCl–sucrose system, regardless of the mode of instability. Conversely, for the heat–KCl–sucrose system, achieving satisfactory convergence in the results depends on the mode of instability and necessitates a greater number of collocation points. In particular, when the instability manifests as a stationary mode, a minimum of $M = 30$ points is required, whereas travelling-wave instability demands $M = 60$ points, as outlined in table 1. Comparing our results under the limiting condition of $R_3 = 0$ (i.e. double-diffusive case) with those obtained by Shankar *et al.* (2022) in table 2 reveals a high degree of agreement. This rigorous validation process underscores the reliability of the current computational code.

4.2. *Double-diffusive case*

During the course of the investigation, some interesting results were found for double-diffusive fluid systems and they are presented first to get a clear idea about the present problem. In fact, these findings were not disclosed in any of the previous investigations. Figure 2 shows the evolution of neutral stability curves for different values of R_2 when $R_3 = 0$ for two values of $Le_2 = 1.2307$ (dashed line) and 87.5 (solid line) corresponding to KCl–NaCl and heat–KCl systems, respectively. From the figure, it is observed that the neutral stability curves are closed, comprising either both stationary and travelling-wave modes or only stationary modes, within which the flow is unstable ($c_i > 0$), while outside of which it defines the parametric conditions of linear stability ($c_i < 0$). Furthermore, the instability is possible only in a finite range of negative values of R_2 depending on the value of Le_2. The salient implication of the closed neutral curve is the requirement of two values of R_1 to completely specify the instability of fluid flow. For $Le_2 = 1.2307$, it is evident that the closed neutral stability curve is formed with two segments of consecutively occurring stationary and travelling-wave modes when $R_2 = -1500$ (figure 2*a*). However, for $R_2 = -700$, the closed neutral curve consists of only single portions of stationary and travelling-wave modes, wherein the latter mode is reduced notably (figure 2*b*). With further increasing R_2, the closed neutral curve progressively transitions to encompass only the stationary mode (figure 2*c–f*). Furthermore figure 2(*a–f*) shows the gradual shrinking of the closed neutral curve with

https://doi.org/10.1017/jfm.2024.490 Published online by Cambridge University Press

https://doi.org/10.1017/jfm.2024.490 Published online by Cambridge University Press

$Le_2 = 1.2307,\ Le_3 = 3.5555$ (KCl–NaCl–sucrose system)

	$R_2=-2000,\ R_3=-1000$			$R_2=-2000,\ R_3=1000$			$R_2=2000,\ R_3=-1000$			$R_2=2000,\ R_3=1000$			$R_2=2100,\ R_3=-400$		
M	R_{1c}	a_c	c_c	R_{1c}	a_c	c_c	R_{1c}	a_c	c_c	R_{1c}	a_c	c_c	R_{1c}	a_c	c_c
5	2719.600113	0.038518	0	525.696837	0.020107	0	−1151.161571	0.048331	0	−3744.783541	0.016180	0	−1747.523020	0.376477	±13.586416
10	2728.709991	0.035060	0	562.878736	0.020073	0	−1145.665853	0.044795	0	−3691.365538	0.015907	0	−1729.209148	0.411577	±11.171355
15	2728.709893	0.035060	0	562.880963	0.020073	0	−1145.665785	0.044795	0	−3691.362447	0.015908	0	−1729.210042	0.411616	±11.170905
20	2728.709893	0.035060	0	562.880952	0.020073	0	−1145.665785	0.044795	0	−3691.362474	0.015908	0	−1729.210040	0.411615	±11.170904
25	2728.709893	0.035060	0	562.880952	0.020073	0	−1145.665785	0.044795	0	−3691.362474	0.015908	0	−1729.210040	0.411615	±11.170904

$Le_2 = 87.5,\ Le_3 = 311.1111$ (heat−KCl−sucrose system)

	$R_2=-2000,\ R_3=-1000$			$R_2=-2000,\ R_3=1000$			$R_2=2000,\ R_3=-1000$			$R_2=2000,\ R_3=1000$			$R_2=-1500,\ R_3=1000$		
M	R_{1c}	a_c	c_c	R_{1c}	a_c	c_c	R_{1c}	a_c	c_c	R_{1c}	a_c	c_c	R_{1c}	a_c	c_c
5	1986.903819	0.000704	0	460.658971	0.000227	0	−2309.766719	0.000777	0	−6576.232837	0.000255	0	−121.76703	0.000200	0
10	1968.674910	0.000563	0	520.089185	0.000226	0	−2239.874882	0.000863	0	−6337.918955	0.000211	0	−69.212576	0.000200	0
15	1969.881719	0.000553	0	520.089556	0.000226	0	−2245.820096	0.000859	0	−6336.112594	0.000211	0	−69.208910	0.000200	0
20	1969.881237	0.000553	0	520.089538	0.000226	0	−2245.732488	0.000859	0	−6336.161177	0.000211	0	−244.831605	1.288581	±353.974900
25	1969.881236	0.000553	0	520.089537	0.000226	0	−2245.732428	0.000859	0	−6336.161204	0.000211	0	−135.250307	0.883081	±299.194579
30	1969.881236	0.000553	0	520.089538	0.000226	0	−2245.732428	0.000859	0	−6336.161204	0.000211	0	−120.634557	0.647730	±290.289404
35													−121.753704	0.483030	±288.757514
40													−121.553096	0.474517	±288.531017
45													−121.557075	0.474328	±288.529918
50													−121.557405	0.474319	±288.529942
55													−121.557403	0.474313	±288.529843
60													−121.557403	0.474313	±288.529843

Table 1. Convergence process of the Chebyshev collocation method for selected values of R_2 and R_3 for KCl–NaCl–sucrose and heat–KCl–sucrose aqueous systems.

		Shankar *et al.* (2022) (Galerkin method)		Present study (Chebyshev collocation method)	
Le_2	R_2	R_{1c}	a_c	R_{1c}	a_c
2	50	51.7327	1.2404	51.732699	1.240434
	100	89.5805	0.8644	89.580817	0.864429
	1000	874.0181	0.0884	874.017521	0.088791
10	10	7.9583	1.0248	7.958246	1.024844
	100	71.3754	0.1399	71.375031	0.139980
	1000	712.8887	0.0142	712.889519	0.014068
100	10	6.5863	0.1867	6.586270	0.186710
	100	65.6941	0.0194	65.694321	0.019357
	1000	656.9253	0.0020	656.925830	0.001936

Table 2. Comparison of results with those of Shankar *et al.* (2022) for double-diffusive system ($R_3 = 0$).

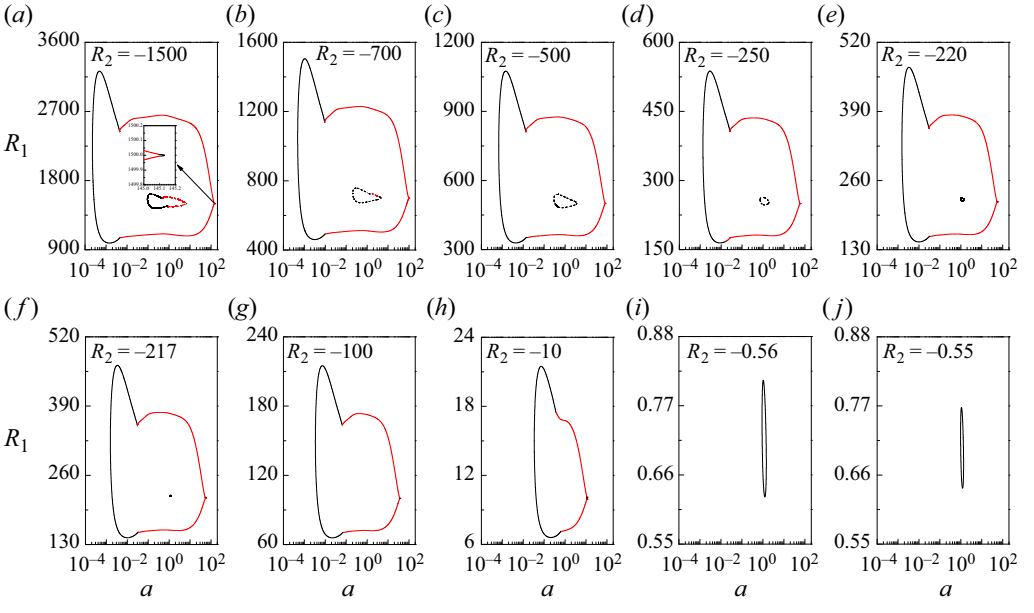


Figure 2. Evolution of neutral stability curves for different negative values of R_2 for double-diffusive system ($R_3 = 0$) when $Le_2 = 87.5$ (solid line) and $Le_2 = 1.2307$ (dashed line). The black and red lines, respectively, denote the stationary and travelling-wave modes and this convention also applies to figures 3–7, 10, 11 and 14–16.

increasing R_2, which eventually collapses into a single point and completely disappears at $R_2 = -216$. Whereas, for $Le_2 = 87.5$, the closed neutral stability curves include two distinct portions of stationary and travelling-wave modes, a pattern extending across a wider range of R_2 (figure 2*a–h*). It is observed that the unstable region gradually decreases with increasing R_2, ultimately vanishing at $R_2 = -0.54$ (figure 2*a–j*). Interestingly, in the current scenario, the range of R_2 within which the instability persists is increased. Besides, the neutral curves of the KCl–NaCl system are encompassed by that of the heat–KCl system with instability occurring at lower wavenumbers in the latter compared

https://doi.org/10.1017/jfm.2024.490 Published online by Cambridge University Press

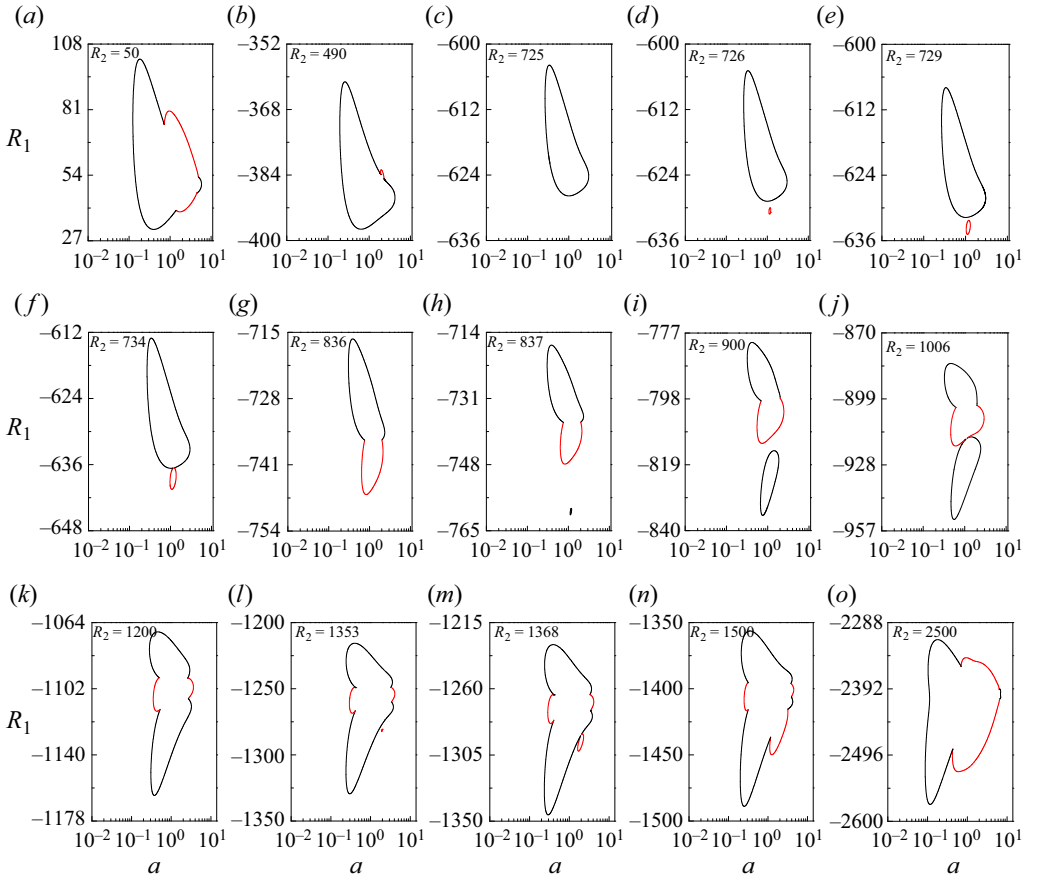


Figure 3. Evolution of neutral stability curves for different positive values of R_2 when $Le_2 = 1.2307$, $Le_3 = 3.5555$ and $R_3 = -100$.

with the former. One common feature observed in all these figures is that the onset of instability arises only through the stationary mode in the case of double-diffusive systems.

4.3. *Triple-diffusive case*

As mentioned earlier, two different sets of transport property ratios are considered in discussing the instability of base flow. The results obtained for these two systems are separately discussed.

4.3.1. *KCl–NaCl–sucrose system (Le_2, $Le_3 \gtrapprox 1$)*

(a) Topology of the neutral stability curves

The impact of a third diffusing component on the progression of neutral stability curves is illustrated in figures 3 and 4, where different values of R_2, spanning both positive and negative domains, are considered when $R_3 = -100$, $Le_2 = 1.2307$ and $Le_3 = 3.5555$. In contrast to the double-diffusive case, the base flow is found to be unstable for both positive and negative values of R_2 and the shape of neutral stability curves is also somewhat unique. For $R_2 = 50$, it is seen that the closed neutral curve is formed by two alternative segments of stationary and travelling-wave modes which exhibit local minimum and the least among

https://doi.org/10.1017/jfm.2024.490 Published online by Cambridge University Press

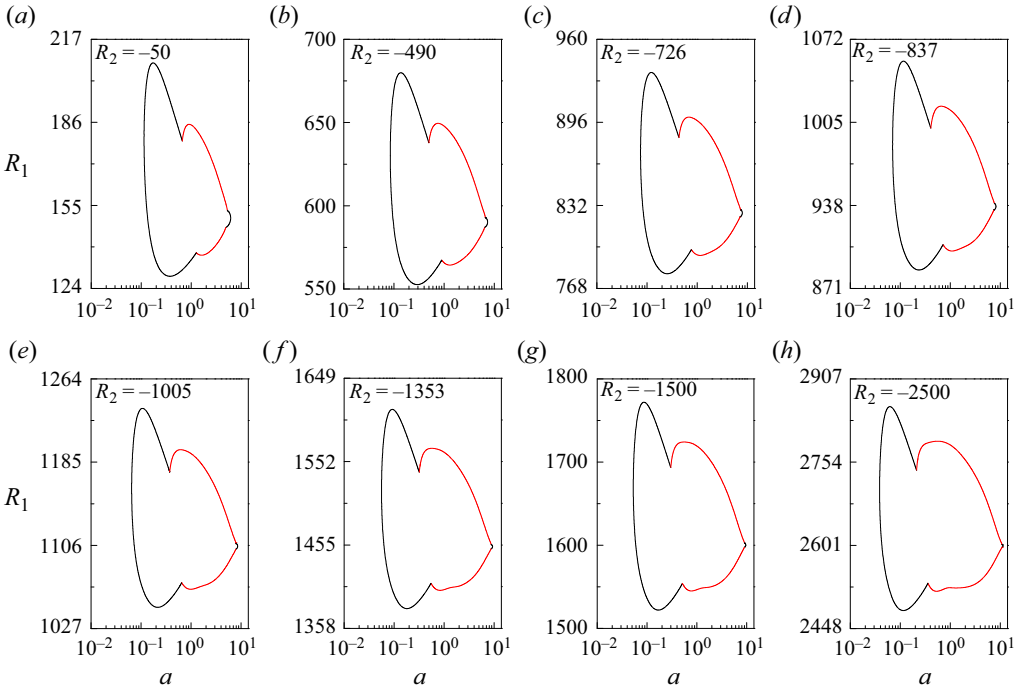


Figure 4. Evolution of neutral stability curves for different negative values of R_2 when $Le_2 = 1.2307$, $Le_3 = 3.5555$ and $R_3 = -100$.

the two corresponds to the stationary mode (figure 3*a*). With increasing R_2, the closed neutral curve progressively simplifies, eventually consolidating into a single segment accommodating both stationary mode and travelling-wave mode, with the latter mode diminishing (figure 3*b*) and even ceasing to exist (figure 3*c*). A noteworthy transformation unfolds at $R_2 = 726$, where both modes manifest as separate closed loops, with the travelling-wave mode positioned beneath the stationary one. This alteration denotes a shift in the mode of instability from the stationary to the travelling-wave mode – an unprecedented finding absent in the context of double-diffusive fluid systems. Such a transition mandates the examination of four R_1 values to comprehensively analyse the fluid flow stability. The disconnected neutral curve pertaining to the travelling-wave mode expands and merges with the stationary neutral curve, thereby evolving into a unified loop with increasing R_2 (figure 3*e–g*). Moreover, a closed loop of the stationary neutral curve emerges below the current loop signifying the reversion of instability to the stationary mode when R_2 reaches the value 837 (figure 3*h*). This closed stationary neutral curve continues to grow (figure 3*i*) until it forms a single loop (figure 3 *j*,*k*). At $R_2 = 1353$, it is seen that yet another closed loop of the travelling-wave mode originates on the right-hand side of the pre-existing loop (figure 3*l*) but it comes together and looms as a single loop with further increase in R_2 (figure 3*m–o*). Throughout this process (figure 3*l–o*), the stationary mode consistently remains the dominant mode of instability even though the instability region varies. In general, the global minimum decreases with increasing R_2. The behaviour of results for negative values of R_2 differs significantly from those obtained for positive values and the same is evident from figure 4. In this figure, the closed neutral stability curves exhibit a consistent pattern, featuring pairs of stationary and travelling-wave modes in succession. In contrast to the previous case, the instability

https://doi.org/10.1017/jfm.2024.490 Published online by Cambridge University Press

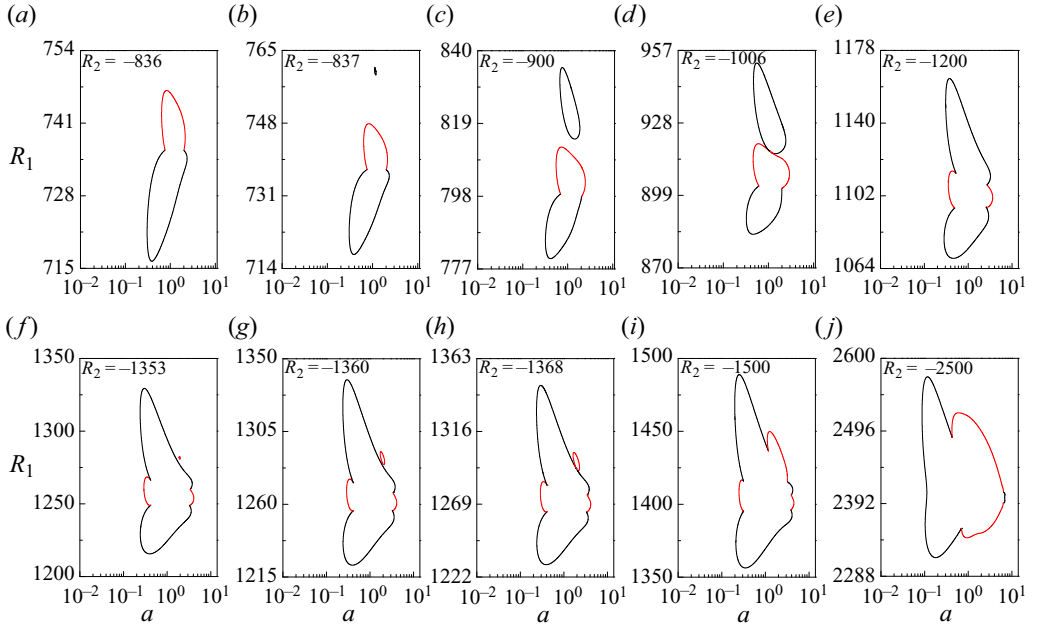


Figure 5. Evolution of neutral stability curves for different negative values of R_2 when $Le_2 = 1.2307$, $Le_3 = 3.5555$ and $R_3 = 100$.

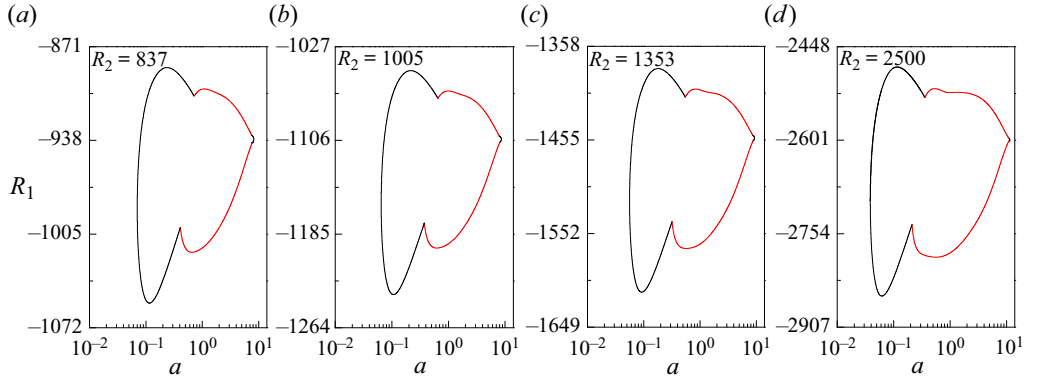


Figure 6. Evolution of neutral stability curves for different positive values of R_2 when $Le_2 = 1.2307$, $Le_3 = 3.5555$ and $R_3 = 100$.

persists exclusively through the stationary mode across all considered values of R_2. Moreover, as R_2 decreases, there is an increase in the instability region and also in the minimum value of R_1.

The neutral curves obtained for $R_3 = 100$, using the same values of R_2, Le_2 and Le_3 as those considered in figures 3 and 4, are showcased in figures 5 and 6 for some isolation cases. The observations reveal a complete reversal of the neutral curves compared with the findings obtained for $R_3 = -100$. A prominent deduction drawn from these visualizations is the unswerving nature of the onset of mode of instability in this particular context, which consistently assumes the form of the stationary mode. This is because, regardless of the values of R_2, when $R_3 = -100$, the maximum value of R_1 reached on the closed neutral curve corresponds to the stationary mode.

https://doi.org/10.1017/jfm.2024.490 Published online by Cambridge University Press

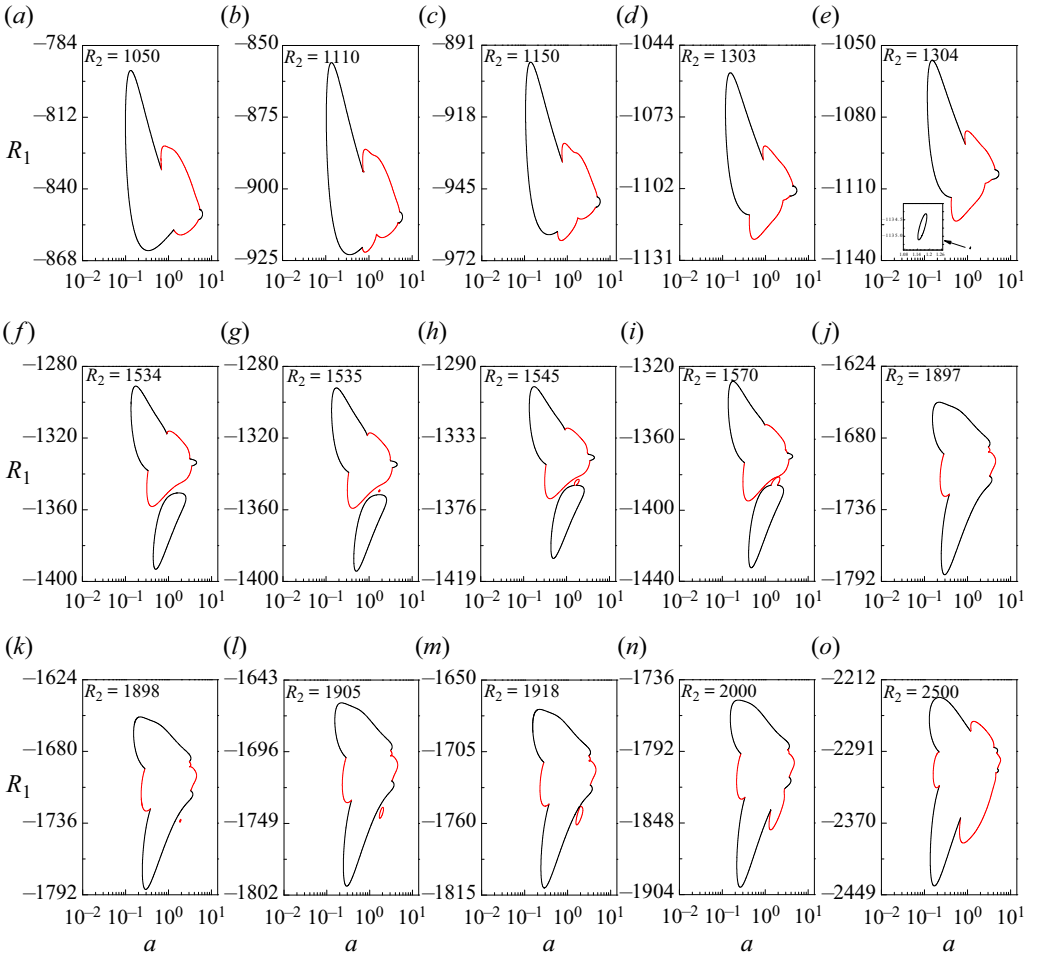


Figure 7. Evolution of neutral stability curves for different positive values of R_2 when $Le_2 = 1.2307$, $Le_3 = 3.5555$ and $R_3 = -200$.

Figure 7 presents a comprehensive depiction of the neutral stability curves for different positive values of R_2 when $R_3 = -200$. The neutral curve loop unravels intricate dynamics involving both stationary and travelling-wave modes for $R_2 = 1050$, featuring two minima wherein the stationary mode predominates as the mode of instability (figure 7*a*). Evidencing further complexity, at $R_2 = 1110$, the neutral curve portrays three local minima, with the initial minimum corresponding to the stationary mode and the subsequent two to the travelling-wave mode. Notwithstanding this complex scenario, the mode of instability continues as the stationary mode (figure 7*b*). Intriguingly, as R_2 increases to 1150, a transition emerges, wherein the mode of instability transitions from the stationary mode to the travelling-wave mode (figure 7*c*). A noteworthy change in the nature of the neutral stability curves manifests at $R_2 = 1303$, as they give up their multi-minimum structure, rendering a single minimum that aligns with the travelling-wave mode (figure 7*d*). Of particular interest is the transition observed at $R_2 = 1304$, marked by the emergence of an extra closed loop depicting the stationary mode (figure 7*e*), necessitating the consideration of four critical values of the Darcy–Rayleigh number to assess the stability of the system. Significantly, the stationary mode reasserts itself as

https://doi.org/10.1017/jfm.2024.490 Published online by Cambridge University Press

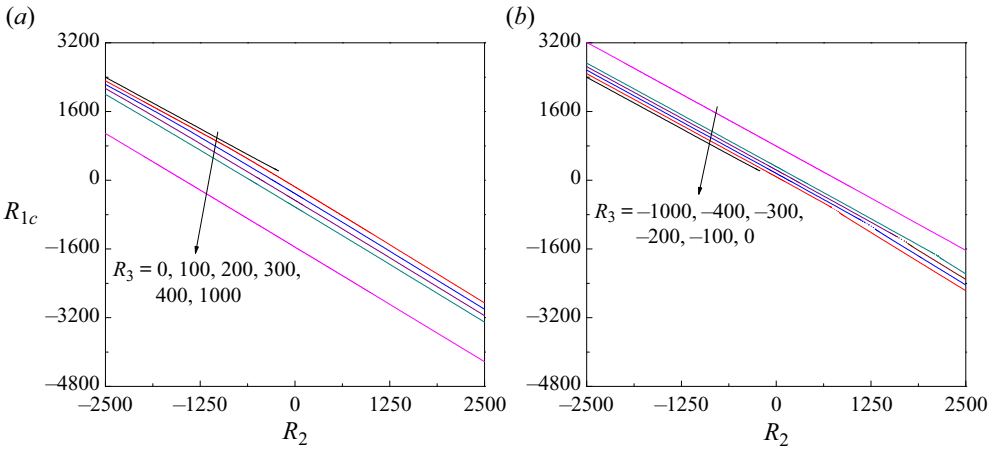


Figure 8. Critical values of R_1 versus R_2 for both positive (a) and negative (b) values of R_3 when $Le_2 = 1.2307$ and $Le_3 = 3.5555$. The solid line represents a stationary mode, while the dotted line corresponds to a travelling-wave mode and this convention is also applicable to figures 9, 12 and 13.

the favoured mode of instability and the closed loop of the stationary mode grows with further increase in R_2 (figure 7f). Importantly, within the intricate interplay of these loops, another closed loop emerges, characterizing the travelling-wave mode (figure 7g). This emergent loop undergoes gradual evolution and subsequently establishes a connection with the lower stationary loop (figure 7h,i), leading to their integration into a coherent single loop (figure 7j) as R_2 progresses. Moreover, yet another closed loop representing the travelling-wave mode appears independently without altering the mode of instability (figure 7k,l) and ultimately amalgamates with the pre-existing closed loop (figure 7m–o). This cumulative loop entails multiple segments, encompassing both stationary and travelling-wave modes. The gradual transformation of these loop structures reveals the complex behaviour of the system in response to varying R_2 values, highlighting the interplay between different modes of instability.

(b) Stability boundaries

The variation of critical Darcy–Rayleigh number R_{1c} as a function of R_2 for different values of R_3 when $Le_2 = 1.2307$ and $Le_3 = 3.5555$ is displayed in figure 8. It is clear that the effect of increasing both R_2 and R_3 is to decrease R_{1c} indicating their effect is to destabilize the fluid flow. For the double-diffusive case ($R_3 = 0$), instability is solely possible through the stationary mode up to $R_2 = -216.08$ and thereafter the flow remains stable. In contrast to this, it is observed that the instability exists for all values of R_2 if the third diffusing component is present. Moreover, the transition of instability changes from the stationary mode (denoted by solid lines) to the travelling-wave mode (denoted by dotted lines) and again reverts back to the stationary mode with increasing R_2, a phenomenon intricately linked to the value of R_3. In particular, the travelling-wave mode instability is present only for negative values of R_3 and it is confined to a finite domain of positive values of R_2 as illustrated in figure 8(b). Also note that this range of R_2 initially increases with decreasing R_3 then starts decreasing and eventually converges to zero as R_3 experiences further reduction. The inherent instability characteristics of fluid flow, manifested across distinct ranges of the parameter R_2, corresponding to different values of R_3, have been discretely tabulated in table 3.

https://doi.org/10.1017/jfm.2024.490 Published online by Cambridge University Press

$Le_2 = 1.2307,\ Le_3 = 3.5555$			
R_3	Stationary	Travelling wave	Stationary
-100	$R_2 \leq 725.23$	$725.23 < R_2 < 836.54$	$R_2 \geq 836.54$
-200	$R_2 \leq 1119.72$	$1119.72 < R_2 < 1303.91$	$R_2 \geq 1303.91$
-300	$R_2 \leq 1594.83$	$1594.83 < R_2 < 1734.86$	$R_2 \geq 1734.86$
-400	$R_2 \leq 2089.38$	$2089.38 < R_2 < 2147.88$	$R_2 \geq 2147.88$

Table 3. Effect of R_3 on the instability transitions from one mode to another in different ranges of R_2 for the KCl–NaCl–sucrose aqueous system.

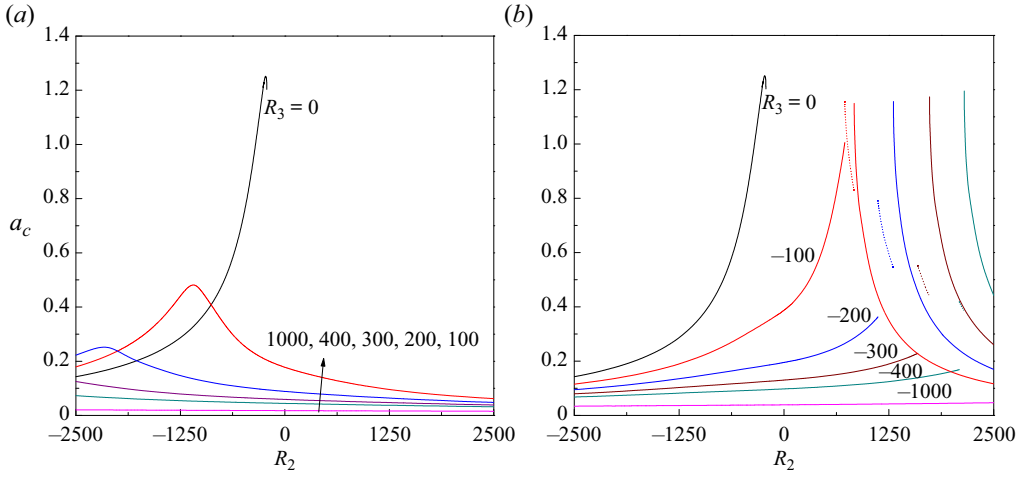


Figure 9. Critical values of a versus R_2 for both positive (a) and negative (b) values of R_3 when $Le_2 = 1.2307$ and $Le_3 = 3.5555$.

The variation of corresponding critical wavenumber a_c with R_2 is presented in figure 9. For positive and also for higher negative values of R_3, no discontinuity in the curves of a_c exists as the instability occurs only through the stationary mode in the considered range of values of R_2. In particular, for $R_3 = 100$ and 200, a_c passes through a maximum value with increasing R_2, while for other positive values of R_3 ($= 300$, 400, 1000), it decreases for all values of R_2 but the trend is found to be not so significant. An entirely distinct scenario becomes visible for negative values of R_3 ($= -100$, -200, -300, -400), a phenomenon attributed to the presence of transition modes, which in turn leads to the emergence of discontinuities in a_c. For $R_3 = -1000$, however, no transition occurs and there is only a slight increase in a_c throughout the range of considered values of R_2. The critical wavenumber corresponding to the stationary mode increases prior to the initiation of the travelling-wave mode, while in post-transition, this a_c value diminishes. It is pertinent to note that within the travelling-wave mode regime, a_c registers a decreasing trend. In the framework of the double-diffusive context ($R_3 = 0$), a_c increases with increasing R_2, reaches the maximum value and then a downturn in a_c follows as R_2 further increases and finally terminates at $R_2 = -216.08$. The critical wave speed c_c increases as R_2 increases; concurrently with a decrease in R_3 values (figures are not shown). Notably, travelling-wave disturbances propagate both upward and downward vertically at the same velocity, owing to the existence of both positive and negative c_c values.

https://doi.org/10.1017/jfm.2024.490 Published online by Cambridge University Press

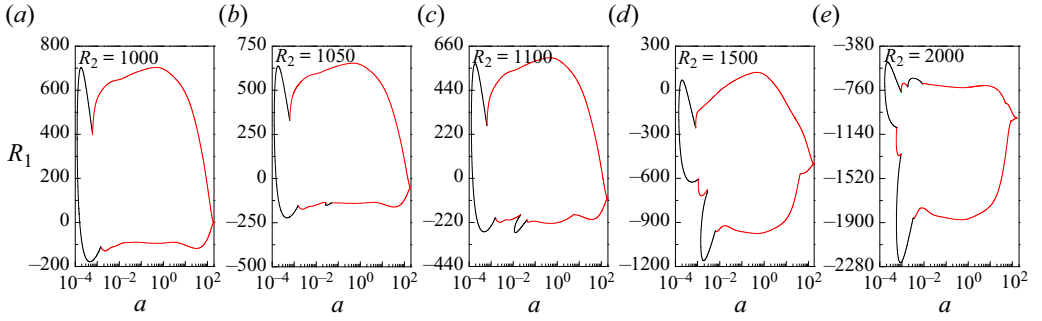


Figure 10. Evolution of neutral stability curves for different positive values of R_2 with $Le_2 = 87.5$, $Le_3 = 311.1111$ and $R_3 = -1000$.

4.3.2. *Heat–KCl–sucrose system* ($Le_2,\ Le_3 \gg 1$)

(a) Topology of the neutral stability curves

The neutral stability curves are shown in figure 10 for different positive values of R_2 when $R_3 = -1000$, $Le_2 = 87.5$ and $Le_3 = 311.1111$. As observed in the previous case, the neutral curves form closed and connected patterns, consisting of both stationary and travelling-wave modes. For $R_2 = 1000$, multiple minima linked to both modes are evident, with primary minimum corresponding to the stationary mode, which is identified as the favoured mode of instability (figure 10*a*). Interestingly, two segments of the neutral stability curve of stationary mode possessing their own local minimum appear for $R_2 = 1050$ and again the instability occurs at the initial wavenumber region (figure 10*b*). Analogously, when $R_2 = 1100$, the neutral stability curves follow the same pattern (figure 10*c*), but the primary instability is now dominated by the local minimum occurring at a higher wavenumber of the stationary mode neutral curve. This particular mode maintains its dominance as the preferred mode of instability even with increased values of R_2 (figure 10*d*,*e*).

Figure 11 portrays the neutral stability curves for different negative values of R_2 when $R_3 = 200$, $Le_2 = 87.5$ and $Le_3 = 311.1111$. We note that a single loop of neutral stability curve featuring multi-minima associated with both modes can be seen with the stationary mode as the preferred mode of instability for $R_2 = -344$ (figure 11*a*). However, an entirely detached closed travelling-wave neutral curve emanates for $R_2 = -343$ which lacks any physical significance for the onset of instability of the system as the minimum R_1 still corresponds to the stationary mode (figure 11*b*). In the subsequent cases, the detached travelling-wave loop gradually expands (figure 11*c*) and eventually merges (figure 11*d–f*) with the pre-existing neutral curve with increasing R_2. Remarkably, during this process, a significant shift takes place in the instability mode, transitioning from the stationary mode to the travelling-wave mode (figure 11*e*). However, as R_2 continues to increase, the system reverts back favouring the stationary mode of instability once again (figure 11*f*).

(b) Stability boundaries

Figures 12 and 13 demonstrate, respectively, the variation of R_{1c} and a_c as a function of R_2 for different values of R_3 when $Le_2 = 87.5$ and $Le_3 = 311.1111$. In the figures, the curve of $R_3 = 0$ corresponds to the double-diffusive system and it is observed that R_{1c} tends to infinity for values of $R_2 > -0.541$ indicating that the flow is always stable, because the perturbations display a negative growth rate. While for values of $R_3 \neq 0$, the instability is found to pervade the entire R_2 domain, as depicted in both panels of figure 12. More specifically, the instability predominantly manifests through the travelling-wave

https://doi.org/10.1017/jfm.2024.490 Published online by Cambridge University Press

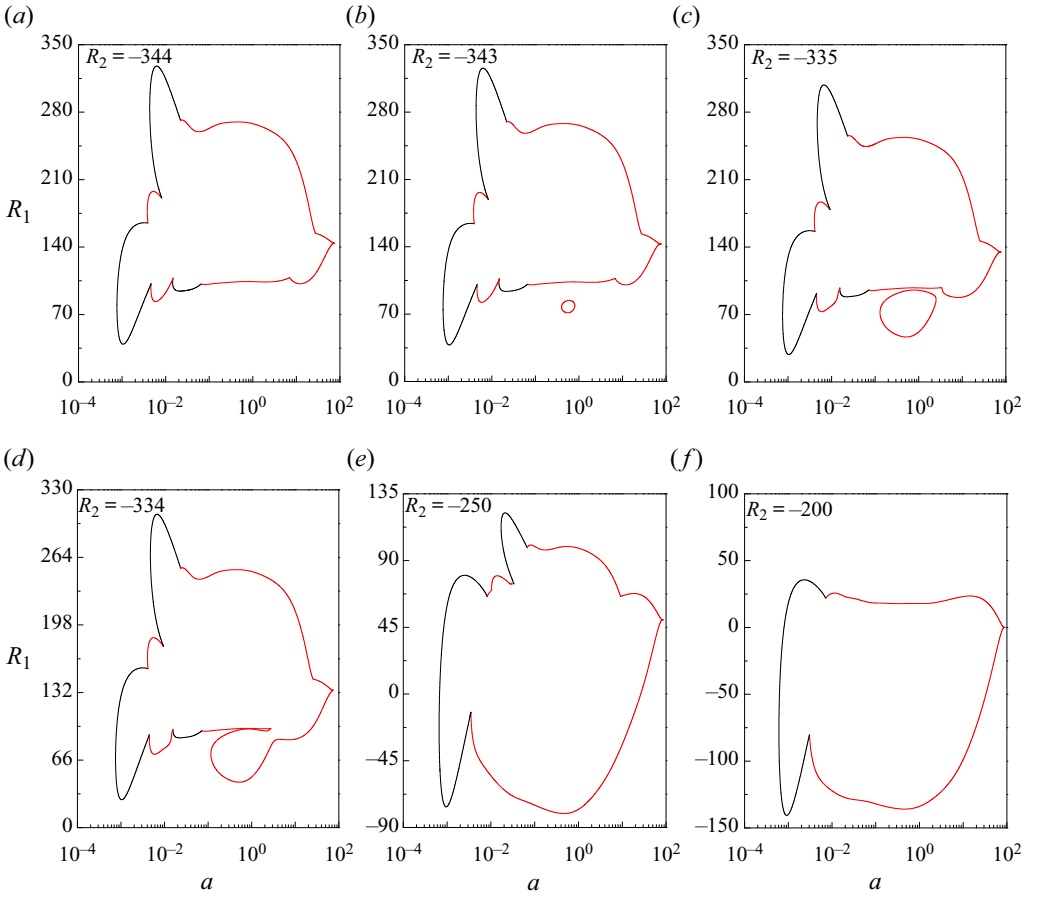


Figure 11. Evolution of neutral stability curves for different negative values of R_2 with $Le_2 = 87.5$, $Le_3 = 311.1111$ and $R_3 = 200$.

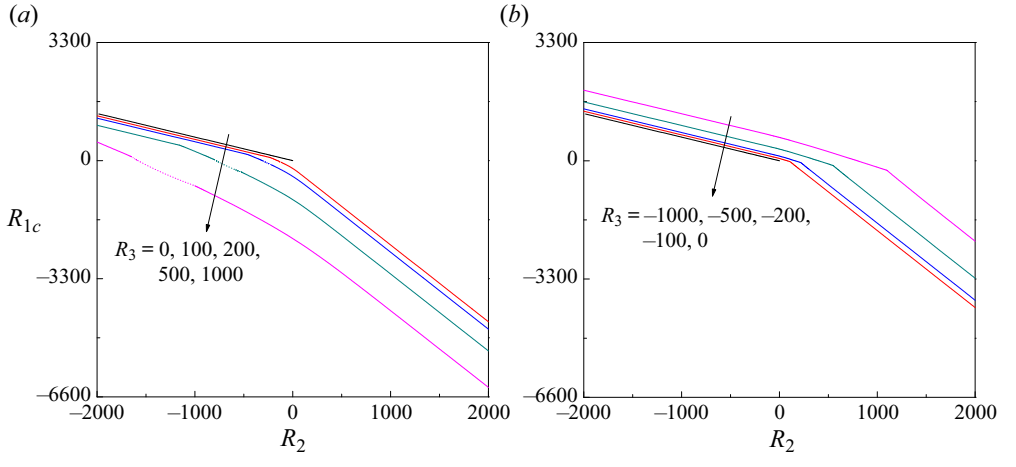


Figure 12. Critical values of R_1 versus R_2 for both positive (a) and negative (b) values of R_3 when $Le_2 = 87.5$ and $Le_3 = 311.1111$.

https://doi.org/10.1017/jfm.2024.490 Published online by Cambridge University Press

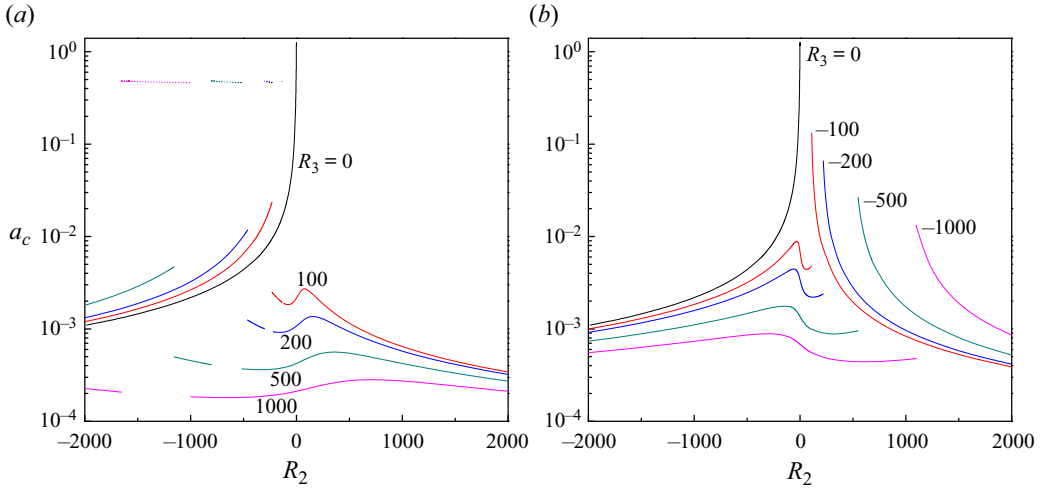


Figure 13. Critical values of a versus R_2 for both positive (a) and negative (b) values of R_3 when $Le_2 = 87.5$ and $Le_3 = 311.1111$.

$Le_2 = 87.5,\ Le_3 = 311.1111$			
R_3	Stationary	Travelling wave	Stationary
100	$R_2 \leq -138.21$	$-138.21 < R_2 < -120.01$	$R_2 \geq -120.01$
200	$R_2 \leq -302.56$	$-302.56 < R_2 < -219.00$	$R_2 \geq -219.00$
500	$R_2 \leq -802.18$	$-802.18 < R_2 < -515.57$	$R_2 \geq -515.57$
1000	$R_2 \leq -1652.49$	$-1652.49 < R_2 < -999.78$	$R_2 \geq -999.78$

Table 4. Effect of R_3 on the instability transitions from one mode to another in different ranges of R_2 for the heat–KCl–sucrose aqueous system.

mode (illustrated by dotted lines) within a specific interval of negative R_2 for positive R_3 values, while in other regimes, instability exclusively arises through the stationary mode (illustrated by solid lines). Additionally, it is noteworthy that the span of R_2 values, where instability is induced through travelling waves, diminishes as R_3 decreases. Moreover, it is worth noting that increasing both R_2 and R_3 serves to speed up the onset of thermoconvective instability in both stationary and travelling-wave modes. The salient observations discussed above are quantified in table 4, providing a comprehensive summary. The critical wavenumber a_c demonstrates distinct trends with increasing values of either R_2 or R_3 (figure 13). A noteworthy observation for positive values of R_3 is the abrupt jump in a_c values within the negative domain of R_2, signifying a pivotal transition in the instability mode from stationary to travelling wave and this behaviour is confirmed quite clearly by the neutral curves displayed in figure 11. Also, during the travelling-wave mode, the variation in a_c becomes relatively less pronounced as R_2 increases. While for negative values of R_3, a sudden variation in a_c curves ensues in the positive domain of R_2 due to the shift in the mode of stationary instability from lower- to higher-wavenumber region (cf. figure 10). The critical wave speed c_c increases proportionally with increased values of R_2 and R_3 (figures are not shown).

https://doi.org/10.1017/jfm.2024.490 Published online by Cambridge University Press

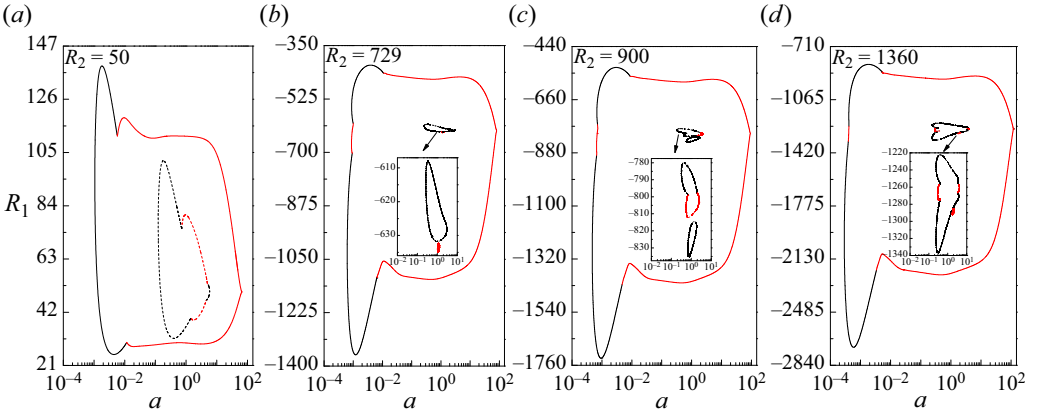


Figure 14. Comparison of neutral stability curves between KCl–NaCl–sucrose (dashed line) and heat–KCl–sucrose (solid line) aqueous systems for different positive values of R_2 with $R_3 = -100$.

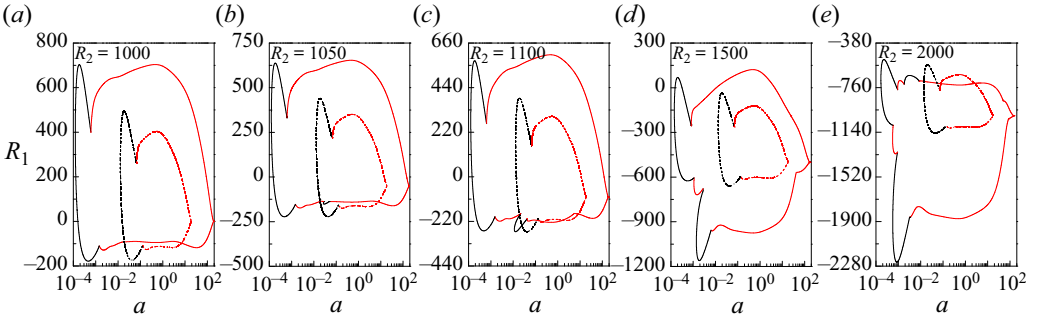


Figure 15. Comparison of neutral stability curves between KCl–NaCl–sucrose (dashed line) and heat–KCl–sucrose (solid line) aqueous systems for different positive values of R_2 with $R_3 = -1000$.

4.3.3. *Comparative study between KCl–NaCl–sucrose and heat–KCl–sucrose systems*

A comprehensive comparative analysis between the KCl–NaCl–sucrose and heat–KCl–sucrose systems has been undertaken to thoroughly understand both the shared characteristics and unique distinctions for the stability of fluid flow. This is facilitated by presenting neutral stability curves in figures 14–16, for identical values of R_2 and R_3. Within these graphical representations, the dashed and solid lines symbolize the KCl–NaCl–sucrose and heat–KCl–sucrose systems, respectively. The neutral curves of the KCl–NaCl–sucrose system either fall comfortably within or intersect with those of the heat–KCl–sucrose system. However, the instability region delineated by the neutral curves of the KCl–NaCl–sucrose system is significantly smaller when compared with the latter system. Additionally, it is observed that the onset of instability happens first in the heat–KCl–sucrose system, no matter what values the governing parameters take. A keen scrutiny of the aforementioned figures also indicates that the transition mode of instability for these two aqueous systems takes place in different regimes of R_2 and R_3. Furthermore, an observation of significance emerges, indicating that the KCl–NaCl–sucrose system necessitates the identification of four critical values of the Darcy–Rayleigh number to establish the linear stability criteria under specific parametric conditions. In stark contrast, the heat–KCl–sucrose system mandates only two critical values for this purpose, irrespective of the values assumed by R_2 and R_3.

https://doi.org/10.1017/jfm.2024.490 Published online by Cambridge University Press

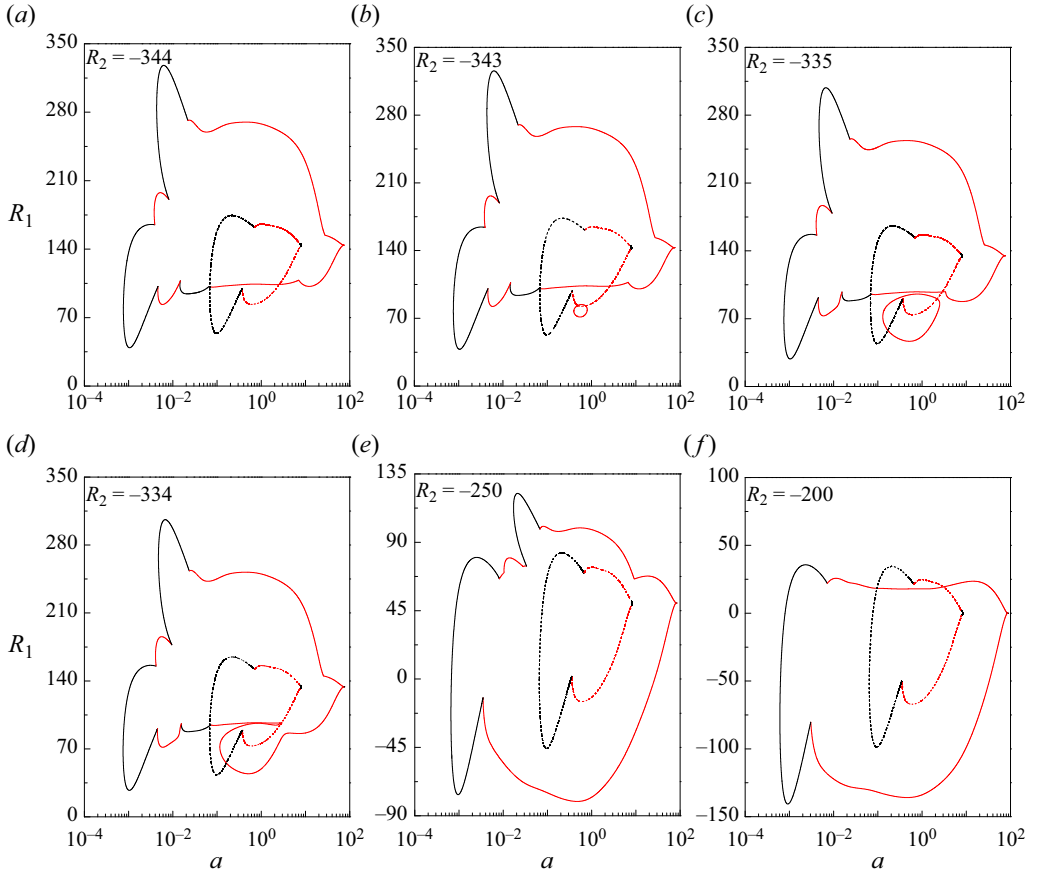


Figure 16. Comparison of neutral stability curves between KCl–NaCl–sucrose (dashed line) and heat–KCl–sucrose (solid line) aqueous systems for different negative values of R_2 with $R_3 = 200$.

5. Conclusions

The linear stability of natural convection in a vertical triple-diffusive fluid-saturated porous layer is investigated. The dynamics of convection is governed by Darcy's law, while the buoyancy effects are characterized by employing the Oberbeck–Boussinesq approximation. A numerical solution of the stability eigenvalue problem has been obtained based on the Chebyshev collocation method for two different transport property ratios relating to KCl–NaCl–sucrose and heat–KCl–sucrose aqueous systems. The evolution of neutral stability curves is examined in detail and it is observed that these two systems exhibit qualitatively different behaviour for the stability of base flow under different regimes of solute Darcy–Rayleigh numbers R_2 and R_3. Besides, the presence of a third diffusing component not only renders the system unstable without any restriction, in contrast to double-diffusive systems, but it also introduces a transition mode that is found to be absent within the ambit of double-diffusive systems.

Some of the novel peculiar features gathered from the foregoing study under different regimes of R_2 and R_3 may be summarized as follows:

(i) When R_2 and R_3 are concurrently positive or negative, the neutral stability curves exhibit a single loop encompassing stationary and travelling-wave modes and the

https://doi.org/10.1017/jfm.2024.490 Published online by Cambridge University Press

instability occurs only through the stationary mode for both the aqueous systems (i.e. no transition mode occurs). Also, two critical values of the Darcy–Rayleigh number are needed to dwell upon the stability criteria. This phenomenon is akin to that observed in double-diffusive fluid systems.

(ii) For values of $R_2 < 0$ and $R_3 > 0$, the possibility of two entirely disjointed neutral curves emerging is found for the KCl–NaCl–sucrose system indicating the necessity of four critical values of the Darcy–Rayleigh number to precisely delineate the stability criteria and the instability exclusively materializes in a stationary mode. On the contrary, the heat–KCl–sucrose system exhibits the sufficiency of two critical values of the Darcy–Rayleigh number for the precise specification of stability criteria despite the neutral curves demonstrating multiple minima and going through a transition mode. The range of R_2 at which the travelling-mode occurs increases with increasing R_3.

(iii) When R_2 takes on positive values and R_3 adopts negative values, the neutral curves are totally disconnected under a certain parametric condition as in (ii) for the KCl–NaCl–sucrose system. Yet, this shift in configuration precipitates a transition in the mode of instability. Specifically, a regime of travelling-wave mode emerges within a defined domain of positive R_2 which progressively diminishes as R_3 decreases further. While for the heat–KCl–sucrose system, only a single loop structure emerges without any transition mode.

Thus the presence of additional diffusing components and the magnitude of transport property ratios assume a pivotal role in delineating the stability characteristics of the system. The instability region outlined by the neutral curves of the KCl–NaCl–sucrose system is notably smaller in contrast to the heat–KCl–sucrose system. Furthermore, the heat–KCl–sucrose system demonstrates greater destabilization compared with the KCl–NaCl–sucrose system. A common feature across both the systems is that increasing the values of either R_2 or R_3 advances the onset of instability, regardless of the mode of instability.

The findings discussed in this study disclose a spectrum of potential avenues for future advancements. One possibility of exploration entails the conceptualization of a sandwiched porous slab, characterized by uniform external layers but varying thermophysical properties within the core layer. This aspect holds significant importance as it offers a deeper insight into convection dynamics in complex configurations. Additionally, a separate research initiative will aim to extend the current work by incorporating the general boundary conditions on velocity, temperature and/or solute concentrations. Another notable concern revolves around the nonlinear stability which may reveal the potential emergence of subcritical instability, providing a valuable comparison to establish the stability threshold.

Acknowledgements. We express our gratitude to the Associate Editor and an anonymous referee for their valuable suggestions, which led to improvements in the manuscript.

Declaration of interests. The authors report no conflict of interest.

Data availability. The data that support the findings of this study are available within the article.

Author ORCIDs.
B.M. Shankar https://orcid.org/0000-0001-8194-537X;
I.S. Shivakumara https://orcid.org/0000-0001-9035-8900.

https://doi.org/10.1017/jfm.2024.490 Published online by Cambridge University Press

References

Anderson, D.M. & Worster, M.G. 1996 A new oscillatory instability in a mushy layer during the solidification of binary alloys. *J. Fluid Mech.* **307**, 245–267.

Barletta, A. 2015 A proof that convection in a porous vertical slab may be unstable. *J. Fluid Mech.* **770**, 273–288.

Barletta, A., Celli, M., Lazzari, S. & Brandão, P.V. 2022 Gill's problem in a sandwiched porous slab. *J. Fluid Mech.* **952**, A32.

Canuto, C., Hussaini, M.Y., Quarteroni, A. & Zang, T.A. 1988 *Spectral Methods in Fluid Dynamics*. Springer.

Celia, M.A., Kindred, J.S. & Herrera, I. 1989 Contaminant transport and biodegradation: 1. A numerical model for reactive transport in porous media. *Water Resour. Res.* **25**, 1141–1148.

Chen, B., Cunningham, A., Ewing, R., Peralta, R. & Visser, E. 1994 Two-dimensional modeling of microscale transport and biotransformation in porous media. *Numer. Meth. Part. Differ. Equ.* **10**, 65–83.

Cheng, P. 1979 Heat transfer in geothermal systems. *Adv. Heat Transfer* **14**, 1–105.

Degens, E.T., von Herzen, R.P., Wong, H.K., Deuser, W.G. & Jannasch, H.W. 1973 Lake Kivu: structure, chemistry and biology of an east African rift lake. *Geol. Rundsch.* **62**, 245–277.

Gershuni, G.Z., Zhukhovitskii, E.M. & Lyubimov, D.V. 1976 Thermal concentration instability of a mixture in a porous medium. *Sov. Phys. Dokl.* **21**, 375–377.

Gill, A.E. 1969 A proof that convection in a porous vertical slab is stable. *J. Fluid Mech.* **35**, 545–547.

Griffiths, R.W. 1979 The influence of a third diffusing component upon the onset of convection. *J. Fluid Mech.* **92**, 659–670.

Griffiths, R.W. 1981 Layered double-diffusive convection in porous media. *J. Fluid Mech.* **102**, 221–248.

Guba, P. & Worster, M.G. 2006 Nonlinear oscillatory convection in mushy layers. *J. Fluid Mech.* **553**, 419–443.

Khan, A.A. & Zebib, A. 1981 Double diffusive instability in a vertical layer of a porous medium. *J. Heat Transfer* **103**, 179–181.

Kwok, L.P. & Chen, C.F. 1987 Stability of thermal convection in a vertical porous layer. *J. Heat Transfer* **109**, 889–893.

Lazzari, S., Celli, M. & Barletta, A. 2021 Stability of a buoyant Oldroyd-B flow saturating a vertical porous layer with open boundaries. *Fluids* **6**, 375.

Moler, C.B. & Stewart, G.W. 1973 An algorithm for generalized matrix eigenvalue problems. *SIAM J. Numer. Anal.* **10**, 241–256.

Nagamani, K.V., Shankar, B.M. & Shivakumara, I.S. 2023 The Prandtl-Darcy convection in a vertical porous layer may be unstable with internal heating. *Transp. Porous Med.* **148**, 417–431.

Naveen, S.B., Shankar, B.M. & Shivakumara, I.S. 2020 Finite Darcy-Prandtl number and maximum density effects on Gill's stability problem. *J. Heat Transfer* **142**, 102601.

Nield, D.A. & Bejan, A. 2017 *Convection in Porous Media*, 5th edn. Springer.

Peyret, R. 2002 *Spectral Methods for Incompressible Viscous Flow*. Springer.

Phillips, O.M. 1991 *Flow and Reaction in Permeable Rocks*. Cambridge University Press.

Poulikakos, D. 1985 The effect of a third diffusing component on the onset of convection in a horizontal porous layer. *Phys. Fluids* **28**, 3172–3174.

Pritchard, D. & Richardson, C.N. 2007 The effect of temperature-dependent solubility on the onset of thermosolutal convection in a horizontal porous layer. *J. Fluid Mech.* **25**, 59–95.

Raghunatha, K.R., Shivakumara, I.S. & Shankar, B.M. 2018 Weakly nonlinear stability analysis of triple diffusive convection in a Maxwell fluid saturated porous layer. *Appl. Math. Mech.* **39**, 153–168.

Rees, D.A.S. 1988 The stability of Prandtl–Darcy convection in a vertical porous layer. *Intl J. Heat Mass Transfer* **31**, 1529–1534.

Rees, D.A.S. 2011 The effect of local thermal nonequilibrium on the stability of convection in a vertical porous channel. *Transp. Porous Med.* **87**, 459–464.

Rionero, S. 2012 Global nonlinear stability for a triply diffusive convection in a porous layer. *Contin. Mech. Thermodyn.* **24**, 629–641.

Rionero, S. 2013 Triple diffusive convection in porous media. *Acta Mech.* **224**, 447–458.

Rudraiah, N. & Vortmeyer, D. 1982 The influence of permeability and of a third diffusing component upon the onset of convection in a porous medium. *Intl J. Heat Mass Transfer* **25**, 457–464.

Scott, N.L. & Straughan, B. 2013 A nonlinear stability analysis of convection in a porous vertical channel including local thermal nonequilibrium. *J. Maths Fluid Mech.* **15**, 171–178.

Shankar, B.M., Kumar, J. & Shivakumara, I.S. 2017 Stability of natural convection in a vertical layer of Brinkman porous medium. *Acta Mech.* **228**, 1–19.

https://doi.org/10.1017/jfm.2024.490 Published online by Cambridge University Press

SHANKAR, B.M., NAGAMANI, K.V. & SHIVAKUMARA, I.S. 2023 Further thoughts on buoyancy-induced instability of a variable viscosity fluid saturating a porous slab. *Phys. Fluids* **35**, 074106.

SHANKAR, B.M., NAVEEN, S.B. & SHIVAKUMARA, I.S. 2022 Stability of double-diffusive natural convection in a vertical porous layer. *Transp. Porous Med.* **141**, 87–105.

SHANKAR, B.M. & SHIVAKUMARA, I.S. 2017 On the stability of natural convection in a porous vertical slab saturated with an Oldroyd-B fluid. *Theor. Comput. Fluid Dyn.* **31**, 221–231.

SHANKAR, B.M. & SHIVAKUMARA, I.S. 2022 Gill's stability problem may be unstable with horizontal heterogeneity in permeability. *J. Fluid Mech.* **943**, A20.

SHANKAR, B.M., SHIVAKUMARA, I.S. & NAVEEN, S.B. 2021 Density maximum and finite Darcy–Prandtl number outlooks on Gill's stability problem subject to a lack of thermal equilibrium. *Phys. Fluids* **33**, 124108.

SHIVAKUMARA, I.S. & RAGHUNATHA, K.R. 2022 Changes in the onset of double-diffusive local thermal nonequilibrium porous convection due to the introduction of a third component. *Transp. Porous Med.* **143**, 225–242.

STRAUGHAN, B. 1988 A nonlinear analysis of convection in a porous vertical slab. *Geophys. Astrophys. Fluid Dyn.* **42**, 269–275.

STRAUGHAN, B. 2015 Convection with local thermal non-equilibrium and microfluidic effects. In *Advances in Mechanics and Mathematics*, vol. 32. Springer.

TRACEY, J. 1996 Multi-component convection-diffusion in a porous medium. *Contin. Mech. Thermodyn.* **8**, 361–381.

https://doi.org/10.1017/jfm.2024.490 Published online by Cambridge University Press